

Understanding Turbulence in Thermal Convection

Abhishek Kumar^a and Mahendra K. Verma^{a,1}

^aDepartment of Physics, Indian Institute of Technology Kanpur, Kanpur, India 208016.

Turbulent convection plays an important role in planetary and stellar flows, as well as in variety of engineering applications. But its understanding and modeling is still far from complete. In this article we perform numerical simulation of turbulent convection in a cube with no-slip boundary condition at all the walls. We observe that the three-dimensional velocity field yields Kolmogorov's spectrum ($k^{-5/3}$). We also record the velocity and temperature time series at several real space probes, just as in experiment. The corresponding frequency spectrum also follows Kolmogorov's spectrum ($f^{-5/3}$), which is because of the Taylor's hypothesis coming into play due to the *steady* large scale circulation. Such application may not be applicable in cylindrical convection due to unsteady azimuthal movements of large scale circulation. Experiments provide limited access to the flow field that makes the deduction of the flow dynamics and energy spectrum difficult. The aforementioned findings based on real space probes provide valuable direction for experimental measurements so as to model convective turbulence.

Thermal convection exhibits a wide range of phenomena—instability, patterns, chaos, and turbulence depending on the strength of the buoyancy force. An idealised system called *Rayleigh Bénard convection* (RBC) (1-3) in which a thin layer of fluid is heated from below and cooled from the top captures the aforementioned complexity. Turbulent convection, a topic of this article, remains largely unsolved despite a century of efforts.

For isotropic fluid turbulence, Kolmogorov (4) showed that one-dimensional energy spectrum $E(k) = C\varepsilon^{2/3}k^{-5/3}$ for intermediate range of wavenumbers (k). Here ε is the energy flux, and C is the Kolmogorov's constant. For buoyancy-driven

turbulence with stable stratification, Bolgiano (5) and Obukhov (6) argued that $E(k) \sim k^{-11/5}$ for the velocity field and $E_T(k) \sim k^{-7/5}$ for the temperature field in the intermediate range of wavenumbers, but Kolmogorov's spectrum for subsequent range of wavenumbers. The steepening of the velocity spectrum compared to Kolmogorov's theory is due to the conversion of the kinetic energy to the potential energy.

Significance

Kolmogorov's spectrum $E(k) \sim k^{-5/3}$ provides a good description for homogeneous, isotropic, and steady fluid turbulence. But a good understanding of the energy spectrum for turbulent convection still lacking. In this paper we report numerical results of convective turbulence in a cube with real space probes and show that both wavenumber and frequency spectra exhibit Kolmogorov's spectrum. Experimental deduction of physics of turbulent convection are more difficult than ones for fluid turbulence due to the lack of a mean flow that puts doubt on the application of Taylor's hypothesis. Our results show that Taylor's hypothesis is applicable to turbulent convection in a cube due to the large scale circulation present in the flow.

Author Contributions: A.K. performed the numerical simulations. M.K.V. wrote the manuscript. A.K and M. K. V. analysed the data.

The authors declare no conflict of interest.

¹To whom correspondence should be addressed. Email: mkv@iitk.ac.in.

Later Procaccia and Zeitak (7) and L'vov and Falkovich (8) generalised the above phenomenology to RBC. Several experiments (9-16) and numerical simulations (17,18) support the Bolgiano and Obukhov phenomenology. However, some others

(19-21) report Kolmogorov's spectrum for RBC. Recently Kumar *et al.* (21) showed that the thermal energy feeds the kinetic energy, hence the energy transfer in RBC differs from stably-stratified flows. This process leads to a Kolmogorov-like spectrum for RBC.

To probe turbulence in thermal convection, scientists measure and analyse the velocity and temperature fields in experiments. The determination of the energy spectrum $E(k)$ requires complete three-dimensional high-resolution real-space data, which is very difficult to record at present. Only a handful experiments enable two-dimensional (2D) visualisation using 2D particle image velocimetry (16, 22-24); an approximate energy spectrum is computed from such data under the assumption of homogeneity and isotropy, which is not strictly valid in convection. In most experiments, the velocity field, $u_z(t)$, and/or temperature field, $T(t)$, are probed at fixed points in the flow (9-15).

In fluid moving with a constant velocity \mathbf{U}_0 , Taylor's hypothesis (25) is invoked to relate the frequency power spectrum $E(f) = |u_z(f)|^2/2$ to one-dimensional wavenumber spectrum $E(k)$ using $E(f) = E(k)(2\pi)/U_0$ since $f = U_0k/(2\pi)$. In supplementary information (SI), we show that $E(k) \sim k^{-5/3}$ and $E(f) \sim f^{5/3}$ in accordance with Taylor's hypothesis. However, for homogeneous and isotropic turbulence with $\mathbf{U}_0 = 0$, we show that $E(f) \sim f^{-2}$ since $f \sim \varepsilon^{1/3}k^{2/3}$ from Kolmogorov's theory (26).

Unfortunately, convective flows do not have a mean velocity \mathbf{U}_0 , hence an application of Taylor's hypothesis to convective turbulence has been intensely debated (2,3). Researchers (9-13) measured the temperature field using real space probes in turbulent convection and reported power spectra with spectral exponents as $-7/5$ in some experiments, and $-5/3$ in others. Niemela *et al.* (14) report dual scaling, as predicted by Bolgiano and Obukhov. There are similar variations in the velocity field exponent as well (15). The uncertainty on the applicability of Taylor's hypothesis to turbulent convection compounds the difficulty in deducing $E(k)$ for the same. He *et al.* (27) employed elliptic model (28) to deduce that the

frequency spectrum of the temperature field $E_T(f) \sim f^{-1.35}$ due to combined effects of sweeping by the random velocity superposed on a mean velocity field. Bershadskii *et al.* (29) obtained $E_T(f) \sim f^{-1.37}$ which they relate to the Clusterization and intermittency.

In this paper we show that in thermal convection, Taylor's hypothesis can be employed to the probe measurements near the walls *only* when a *steady large scale circulation* (30-34) is present in the flow.

Numerical Simulation of Rayleigh Bénard Convection

The dynamical equation that describe RBC under Boussinesq approximation are

$$\frac{\partial \mathbf{u}}{\partial t} + (\mathbf{u} \cdot \nabla) \mathbf{u} = -\nabla p + T \hat{z} + \sqrt{\frac{\text{Pr}}{\text{Ra}}} \nabla^2 \mathbf{u}, \quad [1]$$

$$\frac{\partial T}{\partial t} + (\mathbf{u} \cdot \nabla) T = \frac{1}{\sqrt{\text{RaPr}}} \nabla^2 T, \quad [2]$$

$$\nabla \cdot \mathbf{u} = 0, \quad [3]$$

where \mathbf{u} and T are the velocity and temperature fields respectively, and \hat{z} is the buoyancy direction. The two nondimensional control parameters are the Prandtl number Pr , the ratio of the kinematic viscosity ν and the thermal diffusivity κ , and the Rayleigh number $\text{Ra} = \alpha g \Delta d^3 / (\nu \kappa)$. Here α is the thermal expansion coefficient, Δ and d are the temperature difference and the distance between the plates. Equations [1]-[3] have been nondimensionalized using d as the length scale, $(\alpha g \Delta d)^{1/2}$ as velocity scale, and Δ as the temperature scale.

Equations [1]-[3] are solved in a closed cubical box of unit dimension using an open-source finite-volume code OpenFOAM (35). We employ the no-slip boundary condition for the velocity field at all the walls, conducting boundary conditions for the temperature field at the horizontal wall, and insulating boundary condition at the vertical wall. The grid resolution of our simulation is 100^3 . We make a nonuniform mesh with a higher concentration of grid points near the boundaries in order to resolve the boundary layer (34). We use second-order Crank-Nicolson scheme for time stepping.

We perform our simulation for $Pr = 1$ and $Ra = 10^8$. The Reynolds number Re for this run is approximately 1500. An important response parameter for the convective turbulence is the Nusselt number, which is the ratio of the total (convective plus conductive) heat flux to the conductive heat flux. For the aforementioned simulation $Nu \approx 31.1$.

Wavenumber Spectrum and Structures of RBC

We interpolate the real space simulation data to a uniform mesh of 100^3 grids, and then perform FFT and wavenumber energy spectrum ($E(k)$) computations. Fig. 1A demonstrates that the spectrum is Kolmogorov-like, $E(k) = C\varepsilon^{2/3}k^{-5/3}$, with $C \approx 1.6$. We also compute the energy flux using the Fourier modes. The energy flux $\Pi(k)$ plotted in Fig. 1B shows a constant flux in the inertial range. Thus, our simulation exhibits Kolmogorov's scaling for RBC (21, 36).

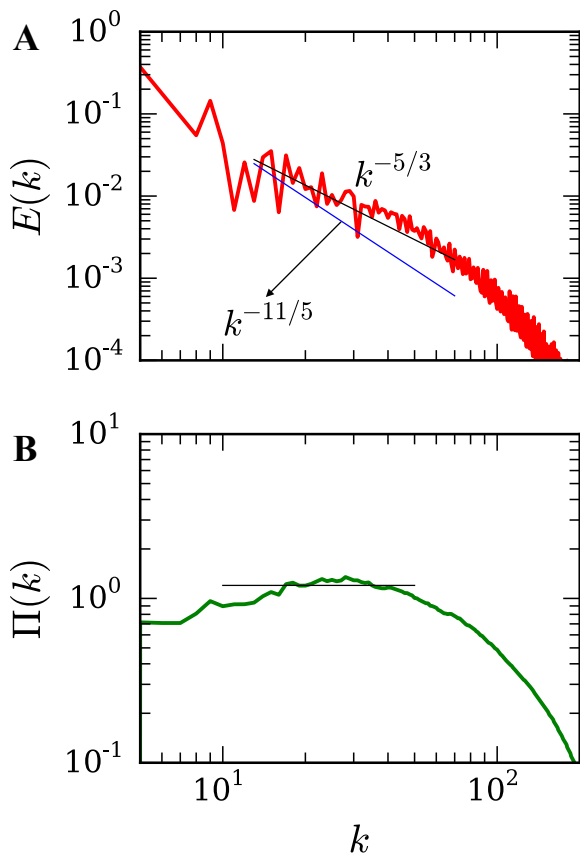


Fig. 1. For RBC with Prandtl number $Pr = 1$ and Rayleigh number $Ra = 10^8$: (A) the kinetic energy spectrum $E(k)$ with $k^{-5/3}$ being a better fit than $k^{-11/5}$; (B) the kinetic energy flux $\Pi(k)$.

Thermal plumes and large-scale structures are prominent in thermal convection. A snapshot of the flow structure in Fig. 2A exhibits ascending hot plumes (red) and descending cold plumes (blue). To obtain further details we analyse the flow velocity at different sections. The three vertical sections exhibited in Fig. 2 B-D clearly demonstrate a *large scale circulation* (LSC) (30-34) with two sets of dominant rolls: in the first roll shown in Fig. 2B, the hot plumes ascend along the right wall, and the cold plumes descend along the left wall; in the second roll shown in Fig. 2C, the aforementioned process occurs along the front and back walls. These two rolls are described by the most energetic velocity Fourier modes $(k_x, k_y, k_z) = (1,0,1)$ and $(0,1,1)$ respectively. The next three most energetic Fourier modes are $(1,1,2)$, $(2,1,1)$, and $(1,4,1)$, but their energies are one order of magnitude lower than those of $(1,0,1)$ and $(0,1,1)$ modes.

Note that the superposition of these modes lead to a strong flow profile for the diagonal plane of Fig. 2D, but a weak flow profile on the opposite diagonal. The steady LSC is also evident in the videos 1 and 2 of the Supplement. The presence of LSC suggests that the Taylor's hypothesis may be applicable to turbulent convection. In the next section we discuss these issues.

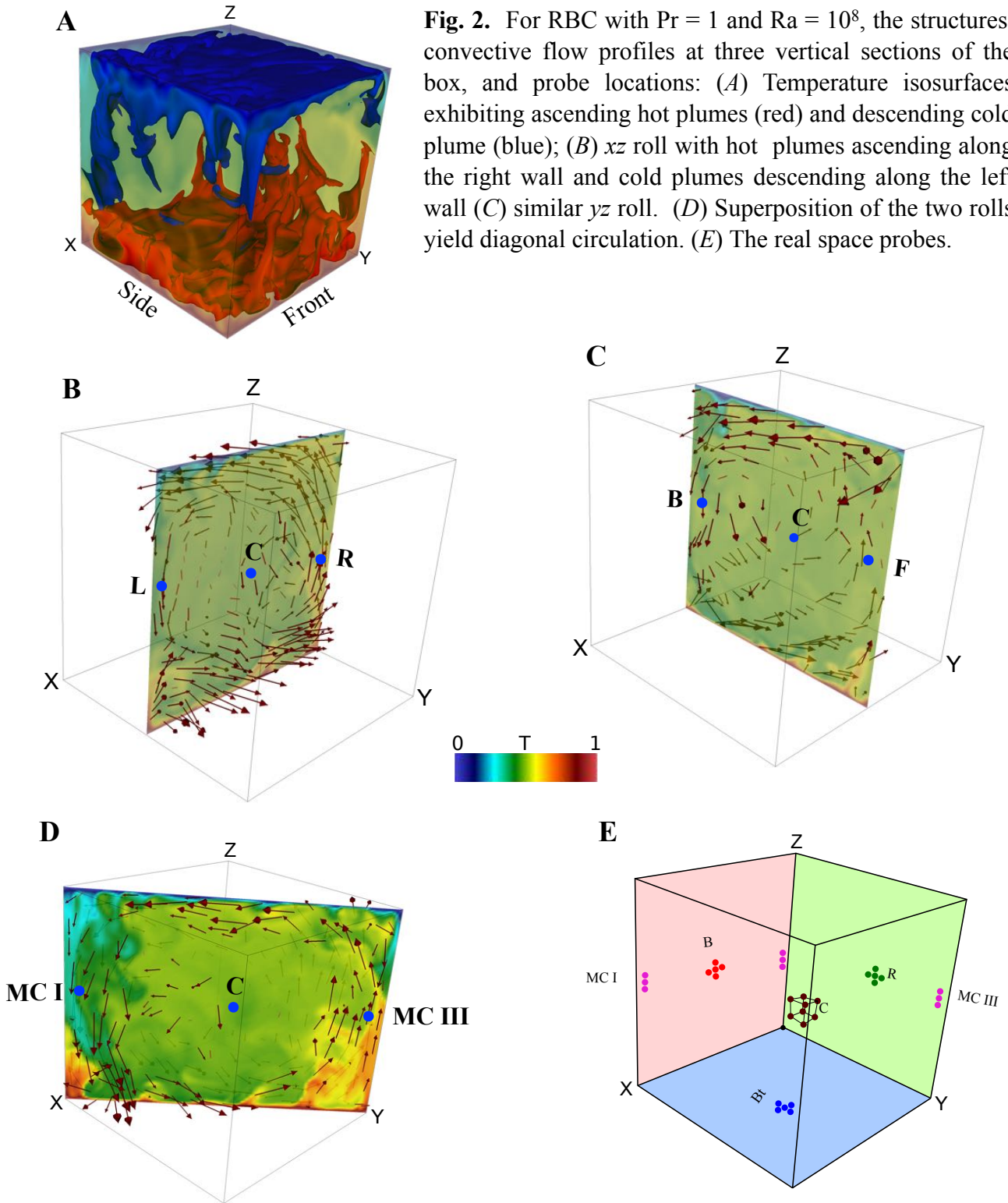
Frequency Spectrum of RBC and Taylor's Hypothesis

In a typical RBC experiment, real space probes are placed near the walls. To relate our simulations with experiments, we place real space probes near the middle of the six wall, near the middle of the corner edges, and in the middle of the cube. We label these probes as front (F), back (B), left (L), right (R), top (T), bottom (Bt), middle corners (MC-I, MC-II, MC-III, MC-IV), and centre (C) respectively. The number of probes near the wall centres, middle corners, and cubic centres are 5, 3, and 9 respectively. In Fig. 2E we exhibit the probes at B, R, Bt, MC I, MC III, MC IV and C.

We record the vertical velocity field $u_z(t)$ at all the real space probes. In the left column of Fig. 3, we exhibit the time series $u_z(t)$ measured at L, R, F, B, MC-I, MC-III and C (see Fig. 2E). Note that $u_z(t)$ is averaged over all the neighbours, e.g., $u_z(t)$ at B is

averaged over the 5 probes shown in Fig. 2E. Here time is in the units of eddy turnover time. We observe that $u_z(t)$ of the side walls and corners fluctuate around the mean values of the LSC.

However $u_z(t)$ of the centre probes fluctuate around zero, which is due to the absence of any mean velocity at the centre of the cube.



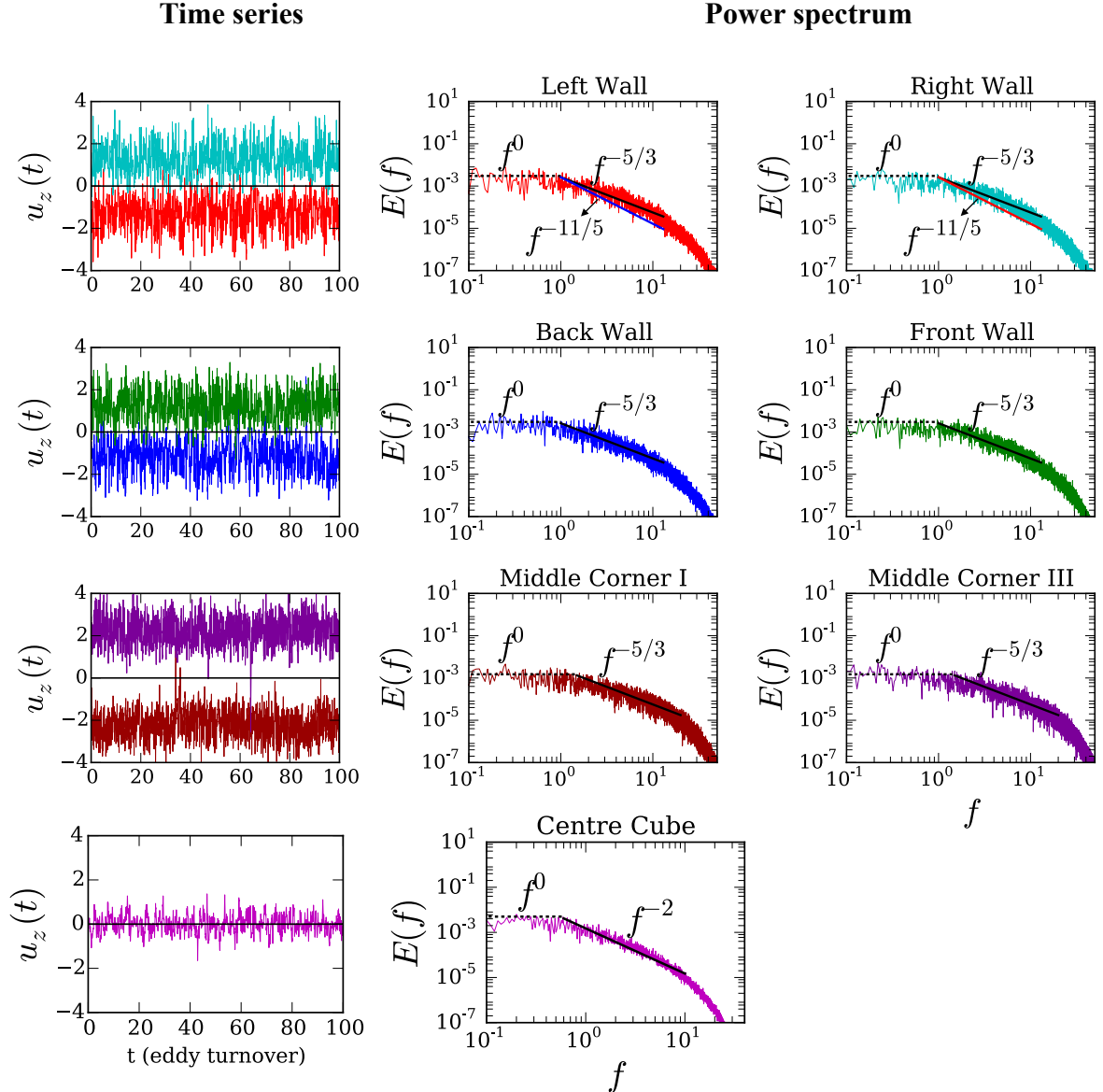


Fig. 3. For RBC with $\text{Pr} = 1$ and $\text{Ra} = 10^8$, time series $u_z(t)$ measured by the probes, and their corresponding frequency spectra. Left panel: time series for the probes at the left-right walls, back-front walls, middle corners I-III, and centre probes (see Fig. 2E). Middle and right panels: The frequency spectrum $E(f)$ computed for the corresponding probes; $E(f) \sim f^{-5/3}$ fits better than $f^{-11/5}$ for the probes at the side walls and middle corners. For the centre of the cube, $E(f) \sim f^{-2}$. Low frequency spectrum $E(f) \sim f^0$ (white noise).

We perform Fourier transform of $u_z(t)$ and compute the frequency spectrum $E(f)$. We observe that $E(f)$ is more noisy than $E(k)$; smoothness of $E(k)$ is due to averaging over the modes of the shells. For the probes at the side walls and mid corners, $E(f) \sim f^{-5/3}$, consistent with the Kolmogorov's phenomenology and Taylor's hypothesis (see middle and right panels of Fig. 3). Here, the LSC acts as carrier of the fluctuations. The centre probe however exhibits $E(f) \sim f^{-2}$ due to the absence of LSC; this result is same as $E(f) \sim f^{-2}$ observed for the fluid turbulence (26) with $U_0 = 0$. Thus we show that Taylor's hypothesis can be employed

to the RBC turbulence only in the presence of a steady LSC.

In the supplement we show that the temperature probes too exhibit similar frequency spectra, though contrast with $f^{-7/5}$ is not very conclusive since $-5/3$ and $-7/5$ are quite close. The difference between the velocity spectral exponents $-5/3$ and $-11/5$ is somewhat larger.

Our results demonstrate the Taylor's hypothesis is applicable to turbulent convection in the presence of a steady LSC. However steady LSC is

not present in many situations. In a cylinder, Niemela et al. (30), Sreenivansan et al. (31), Brown et al. (32), Xi and Xia (33), and Mishra et al. (34) observed azimuthal movement of the LSC, as well flow reversals. Hence, Taylor's hypothesis is questionable for such geometries, and we cannot relate $E(f)$ and $E(k)$ in a straightforward manner. The ambiguities in the earlier experimental results (9-16) are probably due to these reasons. These observations suggest that a usage of a rectangular rather than a cylindrical setup is more appropriate for spectral studies of thermal convection.

Another interesting feature of $E(f)$ is the robust f^0 spectrum (white noise) observed at lower frequencies (see Fig. 3). This feature indicates that the fluctuations at time scales $t \geq 1$ (corresponding to $f \lesssim 1$) are uncorrelated. This behaviour is in sharp contrast to $E(f) \sim f^{-1}$ reported in experiments in flows exhibiting flow reversals (32, 37). The difference is possibly due to the variance of the long-time correlations for reversing and non-reversing velocity signals.

In summary, our numerical simulation of RBC in a cube demonstrates Kolmogorov's spectrum for both wavenumber and frequency spectra. The correspondence between the two spectra is due to the *steady large scale circulation* and the Taylor's hypothesis. Our simulations show that a cubical geometry is better suited than the cylindrical one for spectral studies due to the steady nature of large scale circulation in a cube.

Acknowledgements. We thank Sagar Chakraborty for valuable suggestions. This work was supported by a research grant (Grant No. SERB/F/3279) from Science and Engineering Research Board, India.

1. Chandrashekhara S (1961), *Hydrodynamic and Hydromagnetic Instability* (Oxford University Press, Oxford).
2. Ahlers G, Grossmann S, Lohse D (2009) Heat transfer and large scale dynamics in turbulent Rayleigh-Bénard convection. *Rev Mod Phys* 81:503–537.
3. Lohse D, Xia KQ (2010) Small-scale properties of turbulent Rayleigh-Bénard convection. *Ann Rev Fluid Mech* 42:335–364.

4. Kolmogorov AN (1941) The local structure of turbulence in incompressible viscous fluid for very large Reynolds numbers. *Dokl Akad Nauk SSSR* 30:9-13.
5. Bolgiano R (1959) Turbulent spectra in a stably stratified atmosphere. *Journal of Geophysical Research* 64:2226.
6. Obukhov AN (1959) Effect of Archimedean forces on the structure of the temperature field in a turbulent flows. *Dokl Akad Nauk SSSR* 125:1246.
7. Procaccia I, Zeitak R (1989) Scaling exponents in nonisotropic convective turbulence. *Phys Rev Lett* 62:2128.
8. L'vov VS, Falkovich GE (1992) Conservation laws and two-flux spectra of hydrodynamic convective turbulence. *Physica D* 57:85.
9. Wu XZ, Kadanoff L, Libchaber A, Sano M (1990) Frequency power spectrum of temperature fluctuations in free convection. *Phys Rev Lett* 64:2140.
10. Chillà F, Ciliberto S, Innocenti C, Pampaloni E (1993) Boundary layer and scaling properties in turbulent thermal convection. *Nuovo Cimento D* 15:1229.
11. Cioni S, Ciliberto S, Sommeria J (1995) Temperature structure functions in turbulent convection at low prandtl number. *Europhys Lett* 32:413–418.
12. Zhou SQ, Xia KQ, (2001) Scaling properties of the temperature field in convective turbulence. *Phys Rev Lett* 87:64501.
13. Skrbek L, Niemela JJ, Sreenivasan KR, Donnelly RJ (2002) Temperature structure functions in the Bolgiano regime of thermal convection. *Phys Rev E* 66:036303.
14. Niemela JJ, Skrbek L, Sreenivasan KR, Donnelly RJ (2000) Turbulent convection at very high Rayleigh numbers. *Nature* 404:837.
15. Shang XD, Xia KQ (2001) Scaling of the velocity power spectra in turbulent thermal convection. *Phys Rev E* 64:65301.
16. Sun C, Zhou Q, Xia KQ (2006) Cascades of velocity and temperature fluctuations in buoyancy-driven thermal turbulence. *Phys Rev Lett* 97:144504.
17. Calzavarini E, Toschi F, Tripiccione R (2002) Evidences of Bolgiano-Obukhov scaling in three-dimensional Rayleigh-Bénard convection. *Phys. Rev. E* 66:016304.

18. Verzicco R, Camussi R (2003) Numerical experiments on strongly turbulent thermal convection in a slender cylindrical cell. *J Fluid Mech* 477:19–49.
19. Škandera D, Busse A, and Müller WC (2008) *High Performance Computing in Science and Engineering* (Springer, Berlin) IV:387.
20. Mishra PK, Verma MK (2010) Energy spectra and fluxes for Rayleigh-Bénard convection. *Phys Rev E* 81:056316.
21. Kumar A, Chatterjee AG, Verma MK (2014) Energy spectrum of buoyancy-driven turbulence. *Phys Rev E* 90:023016.
22. Zhou Q, Sun C, Xia KQ (2008) Experimental investigation of homogeneity, isotropy, and circulation of the velocity field in buoyancy-driven turbulence. *J Fluid Mech* 598:361–372.
23. Kunnen RPJ, et al. (2008) Numerical and experimental investigation of structure-function scaling in turbulent Rayleigh-Bénard convection. *Phys Rev E* 77:016302.
24. Zhou Q, Li CM, Lu ZM, Liu YL (2011) Experimental investigation of longitudinal space-time correlations of the velocity field in turbulent Rayleigh-Bénard convection. *J Fluid Mech* 683:94–111.
25. Taylor GI (1938) The spectrum of turbulence. *Proc R Soc Lond A* 164:476.
26. Tennekes H, Lumley JL (1972) *A First Course in Turbulence* (The MIT Press, Cambridge, Massachusetts).
27. He X, He G, Tong P (2010) Small-scale turbulent fluctuations beyond Taylor’s frozen-flow hypothesis. *Phys Rev E* 81:065303(R).
28. He GW, Zhang JB (2006) Elliptic model for space-time correlations in turbulent shear flows. *Phys Rev E* 73:055303(R).
29. Bershadskii A, Niemela JJ, Praskovsky A, Sreenivasan KR (2004) “Clusterization” and intermittency of temperature fluctuations in turbulent convection. *Phys Rev E* 69:056314.
30. Niemela JJ, Skrbek L, Sreenivasan KR, Donnelly RJ (2001) The wind in confined thermal convection. *J Fluid Mech* 449:169
31. Sreenivasan KR, Bershadskii A, Niemela JJ (2002) Mean wind and its reversal in thermal convection. *Phys Rev E* 65:056306.
32. Brown E, Nikolaenko A, Ahlers G (2005) Reorientation of the large-scale circulation in turbulent Rayleigh-Bénard convection. *Phys Rev Lett* 95:084503.
33. Xi HD, Xia KQ (2007) Cessations and reversals of the large-scale circulation in turbulent thermal convection. *Phys Rev E* 75:066307.
34. Mishra PK, De AK, Verma MK, Eswaran V (2011) Dynamics of reorientations and reversals of large-scale flow in Rayleigh-Bénard convection. *J Fluid Mech* 668:480–499.
35. OpenFOAM (2015): The open source CFD toolbox, www.openfoam.org.
36. Kumar A, Verma MK (2015) Shell model for buoyancy-driven turbulence. *Phys Rev E* 91:043014.
37. Hérault J, Pétrélis F, Fauve S (2015) Experimental observation of $1/f$ noise in quasi-bidimensional turbulent flows. *EPL* 111:44002.

Supporting Information

Taylor's Hypothesis in Fluid Turbulence

We performed numerical simulations of three-dimensional fluid turbulence in a static periodic box of dimension $(2\pi)^3$, and in a similar box that is moving with a mean velocity $\mathbf{U}_0 = 10\hat{z}$. The Reynolds number of the flows $\text{Re} = UL/\nu = 1100$, where L , U are respectively the length and velocity scales of the flow, and ν is the kinematic viscosity. In the middle frames of Fig. S1, we illustrate the

vorticity field of a section each of the two boxes at the same time. Fig. S1D is an upward translation by $U_0\tau$, where τ is the time interval, of Fig. S1C, thus indicating a vertical motion of the flow due to \mathbf{U}_0 . We compute the energy $E(k)$ and the energy flux $\Pi(k)$ for both the datasets. As expected, these quantities are identical for both the boxes, and they are plotted in Fig. S1 A and B respectively. In the inertial range we observe Kolmogorov's spectrum.

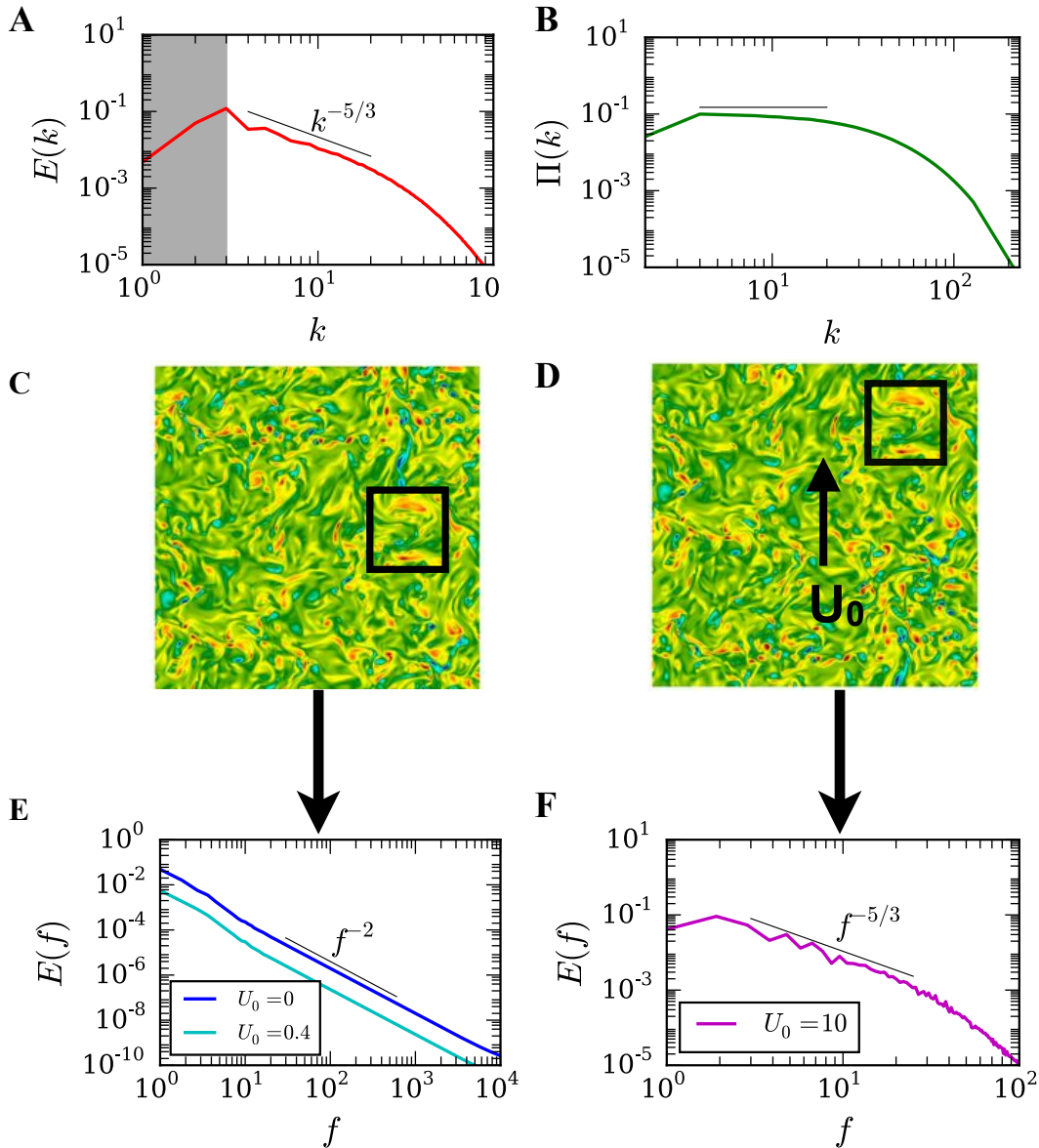


Fig. S1. Fluid turbulence simulation with $\mathbf{U}_0 = 0$ and $\mathbf{U}_0 = 10\hat{z}$, and $\text{Re} = 1100$: (A) energy spectra and (B) energy fluxes are the same for both the flows; they follow Kolmogorov's model. (C, D) The vorticity component ω_x for a vertical cross-section for $U_0 = 0$ and 10 respectively. The flow in D is shifted upward by $U_0\tau$ compared to C. (E) Frequency spectra $E(f) \sim f^{-2}$ for $U_0 = 0$ and 0.4; (F) For $\mathbf{U}_0 = 10\hat{z}$, $E(f) \sim f^{-5/3}$ consistent with Taylor's hypothesis.

We record the time series of the velocity field at 50 random locations, and then compute their frequency spectra $E(f)$. Figures S1 *E* and *F* exhibit the averaged $E(f)$ over the 50 probes for $\mathbf{U}_0 = 0$ and $\mathbf{U}_0 = 10\hat{z}$ respectively. For $\mathbf{U}_0 = 10\hat{z}$, $E(f) \sim f^{-5/3}$, in accordance with Taylor's hypothesis (25) since $2\pi f = U_0 k$. However, for homogeneous and isotropic turbulence with $\mathbf{U}_0 = 0$, we obtain $E(f) \sim f^{-2}$ since $f \sim \varepsilon^{1/3} k^{2/3}$ from Kolmogorov's theory (26). Interestingly, we also observe $E(f) \sim f^{-2}$ for small U_0 when $\varepsilon^{1/3} k^{2/3} > U_0 k$ (see Fig. S1*E* for $\mathbf{U}_0 = 0.4\hat{z}$).

Frequency spectrum for the temperature field of RBC

In Fig. S2 we plot the time series $T(t)$ for some of the thermal probes and their corresponding frequency spectra. We observe that $E_T(f) \sim f^{-5/3}$ is a better fit to the data than $E_T(f) \sim f^{-7/5}$, thus supporting Kolmogorov's spectrum for the RBC (similar to passive scalar). The contrast however is not as conclusive as the velocity spectral indices for which the difference between the two, $-5/3$ and $-11/5$, is larger.

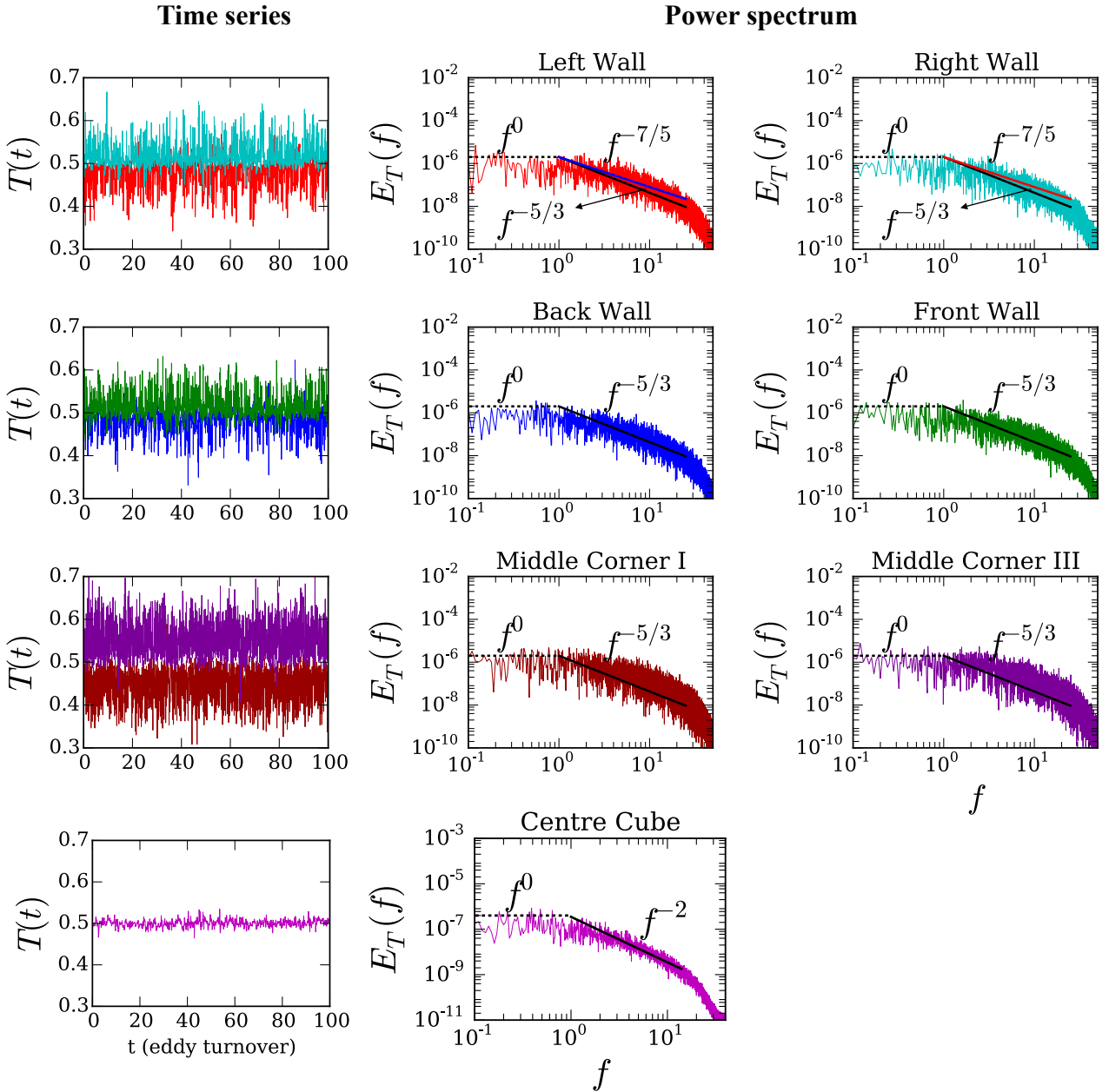


Fig. S2. For RBC with $\text{Pr} = 1$ and $\text{Ra} = 10^8$: Time series of temperature, $T(t)$, measured at various probes and their frequency spectra. Left panel: $T(t)$ for the probes at the left-right walls, back-front walls, middle corners I-III, and at the cube centre (see Fig. 2*E* of the main Text). Middle and right panels: The frequency spectrum $E_T(f)$ computed for the corresponding probes. $E_T(f) \sim f^{-5/3}$ for the probes at the side walls and middle corners, consistent with Taylor's hypothesis and Kolmogorov's theory, but $E_T(f) \sim f^{-2}$ at the centre of the cube.